Human-induced warming accelerates local evapotranspiration and precipitation recycling over the Tibetan Plateau

Check for updates

Tat Fan Cheng [1,2] ✉, Deliang Chen [3], Bin Wang [2], Tinghai Ou [3] & Mengqian Lu [1] ✉

The Tibetan Plateau faces changing precipitation and environmental conditions affecting alpine ecosystems and downstream freshwater sustainability. While aerosol influence has been highlighted, how human-induced greenhouse warming impacts the plateau's moisture recycling remains unclear. Here we show that the Tibetan Plateau's recent precipitation changes result from enhanced precipitation recycling and moisture convergence that offset the decline in monsoon- and westerly-associated moisture transport based on 40-year Lagrangian simulations and water budget analyses. Local evapotranspiration is observed to increase faster in percentage than precipitation, a trend expected to continue in future warming scenarios according to climate projections. Greenhouse gas emission causes widespread wetting while weakening the southerly monsoons across the Himalayas, heightening the sensitivity of precipitation to evapotranspiration and thereby local land surface changes. This trend exacerbates vulnerability in the water cycle of high mountain Asia, calling for proactive management to address potential risks and ensure future water and food security in Asia.

Earning the grand title of Asian water tower, the Tibetan Plateau (TP) serves as the backbone of the region's freshwater supply, food security, and socioeconomic development[1–4]. It gives birth to twelve major river systems in Asia (Fig. 1a) and profoundly influences the health and livelihood of almost two billion people––a quarter of the global population today[2,5]. Most water tower-dependent countries downstream are developing nations with a high vulnerability to water supply disturbance[3,5,6]. The TP is home to the world's most biologically rich but fragile ecosystems, housing over 14,000 alpine plants and 1700 mountain animal species, with a tenth of which are currently endangered or vulnerable[5].

Like many other water towers worldwide, the TP is highly sensitive to climate change[2,7]. With anthropogenic greenhouse gas (GHG) forcing and elevation-dependent warming at work[8], the TP has warmed at over 0.3 K per decade over the past 60 years, far exceeding the global average rate[3,5,9]. A cascade of environmental upheaval has taken place on the TP, including glacial retreat and shrinkage[10], rapid lake expansion[11–13], elevated streamflow[14], permafrost degradation[15–17], and greening[18,19]. Acute drying has been observed along the southeast and northwest Himalayas, impacting the upstream areas of the Indus, Brahmaputra, Irrawaddy, and Mekong basins (Fig. 1b). Meanwhile, conspicuous wetting is observed in a vast part of the inner TP, encompassing the headwater regions of

the Tarim and Yangtze River basins as well as the two endorheic basins where new or expanded water bodies were found[11–13].

Previous studies conjectured the role of the weakening Indian monsoon[20–22] in causing the spatial contrast of precipitation change on the TP. The weakening of the Asian westerly jet was argued to result from uneven emission of anthropogenic aerosol that caused the TP's precipitation change[23]. However, it remains an open question how a weakening westerly jet triggers the inner wetting, for it could disfavor instability and precipitation formation[24]. Further, there lacks concrete, quantitative evidence on how the large-scale circulation changes modified upwind moisture sources and gave rise to the precipitation changes in high mountain Asia. From the moisture recycling standpoint, the warming-induced environmental changes, as mentioned earlier, could give rise to stronger local evapotranspiration flux (Fig. 1c) and feedback to atmospheric conditions and precipitation through land-atmosphere interactions[3,5,10]—a process known as precipitation recycling[25–38]. The latest climate projection indicates that the TP will become increasingly warmer and wetter throughout the 21st century[5,39]. However, how changes in nonlocal and local moisture recycling impact the present and future climate sensitivity of the Asian water tower remains mostly obscure. This impedes the development of optimized water use management and climate resilience strategies for downstream societies in future high mountain Asia.

[1]Department of Civil and Environmental Engineering, The Hong Kong University of Science and Technology, Clear Water Bay, Hong Kong, China. [2]Department of Atmospheric Sciences and International Pacific Research Center, University of Hawai'i at Mānoa, Honolulu, HI, USA. [3]Department of Earth Sciences, University of Gothenburg, Gothenburg, Sweden. ✉e-mail: franklin.cheng@ust.hk; mengqian.lu@ust.hk
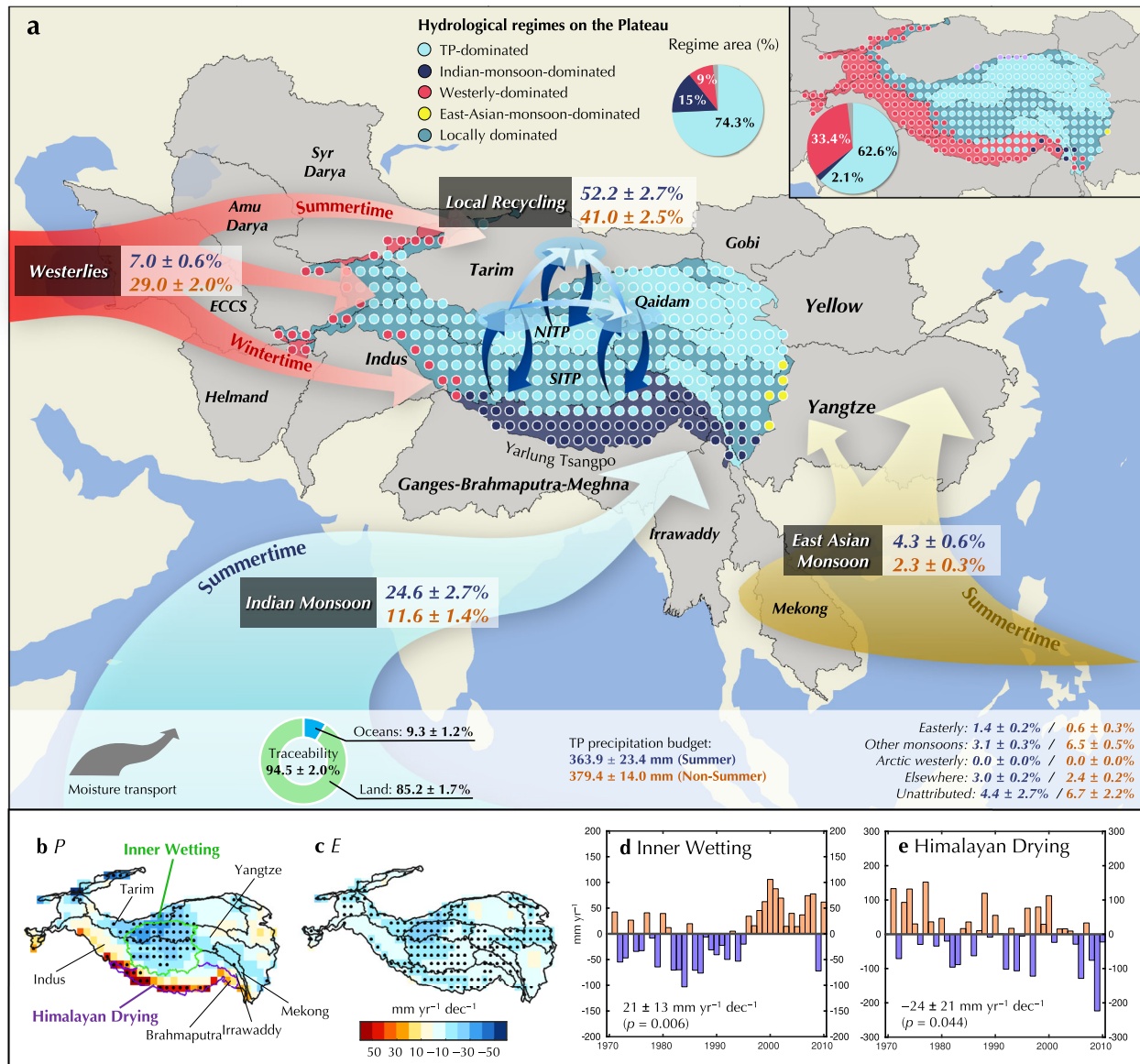
Fig. 1 | Moisture recycling, hydrological regimes, and precipitation changes in the Tibetan Plateau (TP). a The TP (outlined by an altitude of 3000 m) and its river basins. The downstream areas of the basins are shown in grey. ECCS: east coast of the Caspian Sea, NITP: northern inner TP, SITP: southern inner TP. Based on the Lagrangian approach for moisture tracking and regime classification, the ratio contributions (mean ± S.D., unit: %) of precipitation recycling and external moisture conveyors to the summer (June–July–August, JJA) and non-summer precipitation on the TP are shown in blue and orange, respectively. Contributions from other conveyors are listed on the bottom right. The donut chart on the bottom left displays the total moisture traceability and the contributions from the oceans and land by the Lagrangian approach. On the TP, colors of the $1° \times 1°$ grid cells show the summertime dominant moisture conveyors (i.e., hydrological regimes) for the local precipitation. The pie chart shows the fractional coverage (unit: %) of the hydrological regimes with respect to the TP's total surface area. The inset on the top right shows the non-summertime hydrological regimes. **b** A spatial pattern of the trend of the TP precipitation (unit: mm yr^{-1} dec^{-1}) over 1971–2010 based on CERA-20C reanalysis. Stippling denotes the statistically significant trends at the 0.1 level (Mann–Kendall test). **c** Similar to (**b**), but for the evapotranspiration trends. **d** Bar plot showing the inner wetting based on the anomalous precipitation over the NITP and SITP with respect to the climatological mean (1971–2010). The trend and the corresponding p-value (Mann–Kendall test) are shown at the bottom. **e** Similar to (**d**), but for the Himalayan Drying based on precipitation in the Yarlung Tsangpo basin.

Here we seek to untangle the complex interplay of precipitation recycling and moisture advection in the origin of the TP's hydrological changes using a three-dimensional (3D) Lagrangian approach for moisture tracking. We demonstrate that the observed inner wetting is a product of intensified precipitation recycling propelled by stronger evapotranspiration plus enhanced moisture convergence. Drawing from the Coupled Model Intercomparison Project Phase 6 (CMIP6) multi-model single-forcing experiments[40] and climate projections[41], we propose a dual effect of man-made GHG warming on the TP's future hydroclimate: it bolsters precipitation recycling and wetting while concurrently impairing the southerly monsoons across the Himalayas. The TP evapotranspiration is projected to scale effectively faster than precipitation with respect to the GHG-induced rising temperature. These lines of evidence bespeak a burgeoning likelihood that the hydrological cycle over the Asian water tower becomes increasingly self-constrained in a warming climate, with rising sensitivity and vulnerability to local land surface change.

Results

Moisture sources and hydrological regimes of the TP

While considerable attention has been paid to the interaction between local moisture recycling, monsoonal flows, and westerly winds[1,3,42], there is limited research disentangling the relative significance of these

Table 1 | Precipitation recycling ratio of the Tibetan Plateau (TP) reported in previous studies

No.	Study	Method	Framework	Consider cascading effect?	Data	Time	Region	Precipitation recycling ratio	
								Annual	**Summer**
1	Yang et al.[25]	Isotopic analysis	-	-	Water isotope	1997	Three sites in Central TP	-	46.86%
2	Kurita and Yamada[26]	Isotopic analysis	-	-	Water isotope	2004	Naqu, Central TP	-	30–80%
3	An et al.[27]	Isotopic analysis	-	-	Ice-core isotope, ERA-I	1979–2012	Chongce, Central TP	53.2% ± 18%	-
4	Curio et al.[28]	Budget analysis	2D Eulerian	No	HAR	2001–2012	TP	63.2%	42.2–46.4%
5	Zhang et al.[29]	WAM-2layers[a]	2D Eulerian	No	ERA-I	1979–2013	Central TP	18%	-
6	Xu and Gao[30]	QIBT model[b]	2D Eulerian	No	ERA-I	1982–2011	Southeast TP	-	35%
7	Guo et al.[31]	WAM-2layers	2D Eulerian	No	ERA-I	1979–2015	Central TP	26%	24%
8	Zhang[32]	WAM-2layers	2D Eulerian	No	ERA-I	1998–2018	TP	23.6% ± 2.3%	22.1%
9	Zhao et al.[33]	Bulk model	2D Eulerian	No	RCM[f]	2009	TP	-	21–27%
10	Zhao and Zhou[34]	Bulk model	2D Eulerian	No	ERA5	1979–2018	TP	-	23%
11	He et al.[35]	DRM[c]	2D Lagrangian	No	ERA5	1979–2019	TP	-	24%
12	Li X. et al.[36]	Bulk model	2D Eulerian	No	ERA5	1979–2018	TP	12.2%	26.3%
13	Li Y. et al.[37]	WAM-2layers	2D Eulerian	No	ERA-I, MERRA-2, JRA-55	1979–2015	TP basins	~10–20%	-
14	Sun and Wang[46]	FLEXPART-ASRA[d]	3D Lagrangian	Yes	NCEP-CFSR	2000–2009	A tiny box in Northeast TP	6–8%	~8%
15	Gao et al.[38]	WRF-WVT[e]	3D Eulerian	No	ERA-I	2001	TP	10–40%	40%
16	Ma et al.[47]	WRF-WVT	3D Eulerian	No	ERA5	2005–2019	TP	18.9%	23.3%
17	This study	FLEXPART-WaterSip	3D Lagrangian	Yes	CERA-20C	1971–2010	TP	46.5% ± 2.2%	52.2% ± 2.7%

Missing or inapplicable information is denoted with a hyphen.
[a]Water accounting model-2 layers.
[b]Quasi-isentropic backward trajectory model.
[c]Dynamical recycling model.
[d]ASRA: Areal source-receptor attribution method.
[e]Weather Research and Forecasting model with water vapor tracers.
[f]Output from two regional climate model simulations.

factors[43]. Here, we dissect the annual precipitation cycle into summer (June–July–August, JJA) and non-summer seasons (Fig. 1a). In virtue of a 3D Lagrangian tracking model[44] coupled with the WaterSip moisture-source diagnostics[45] (see "Methods" section), we have attributed the source of up to 94.5 ± 2.0% of the TP precipitation year-round. In the summer season, plateau-wide precipitation recycling sustains approximately half (52.2 ± 2.7%) of the total TP precipitation, while its significance noticeably drops to 41.0 ± 2.5% during the non-summer season (Fig. 1a). The uncertainties represent the interannual variabilities of the moisture contributions based on one standard deviation. Throughout the year, precipitation recycling accounts for 46.5 ± 2.2% of the TP precipitation. Our Lagrangian estimate of precipitation recycling ratio aligns well with those based on water and ice-core isotopes (46.9–53.2%)[25,27] but surpasses the estimation range based on 2D/Eulerian tracking, which typically falls between 10% and 40%[25–38,46,47] (see Table 1 and "Discussion" section). The dominant role of precipitation recycling bespeaks an increasingly sensitive hydrological cycle to land surface fluxes and properties over the TP.

The Himalayan precipitation variability is prone to the seasonal interplay between the Indian monsoon and westerlies. By classifying global circulation regimes (see "Methods" section), we determine that the Indian summer monsoon plays a leading role in transporting tropical moisture into the TP, accounting for 24.6 ± 2.7% of the TP summer precipitation (Fig. 1a). The mid-latitude westerlies, on the other hand, contribute as a secondary factor (7.0 ± 0.6%) in summer. Further, our grid-scale moisture tracking experiments confirm that the southern and southeastern Himalayas belong to an Indian monsoon-dominated regime. Driven by the southwesterly monsoons and the cross-equatorial Somali Jet[48,49], the summertime Himalayan precipitation is noticeably fed by a large-scale, meandering aerial waterway through the Yarlung Zangbo Grand Canyon, as revealed by precipitation footprints[50,51] (i.e., the moisture-source field; see "Methods" section; Supplementary Fig. 1).

Contrastingly, during the non-summer months when the subtropical westerly jet restores its intensity and migrates southward following the maximum meridional temperature gradient in the upper troposphere[52,53], it becomes the leading conveyor of external moisture to the TP (29.0 ± 2.0%)
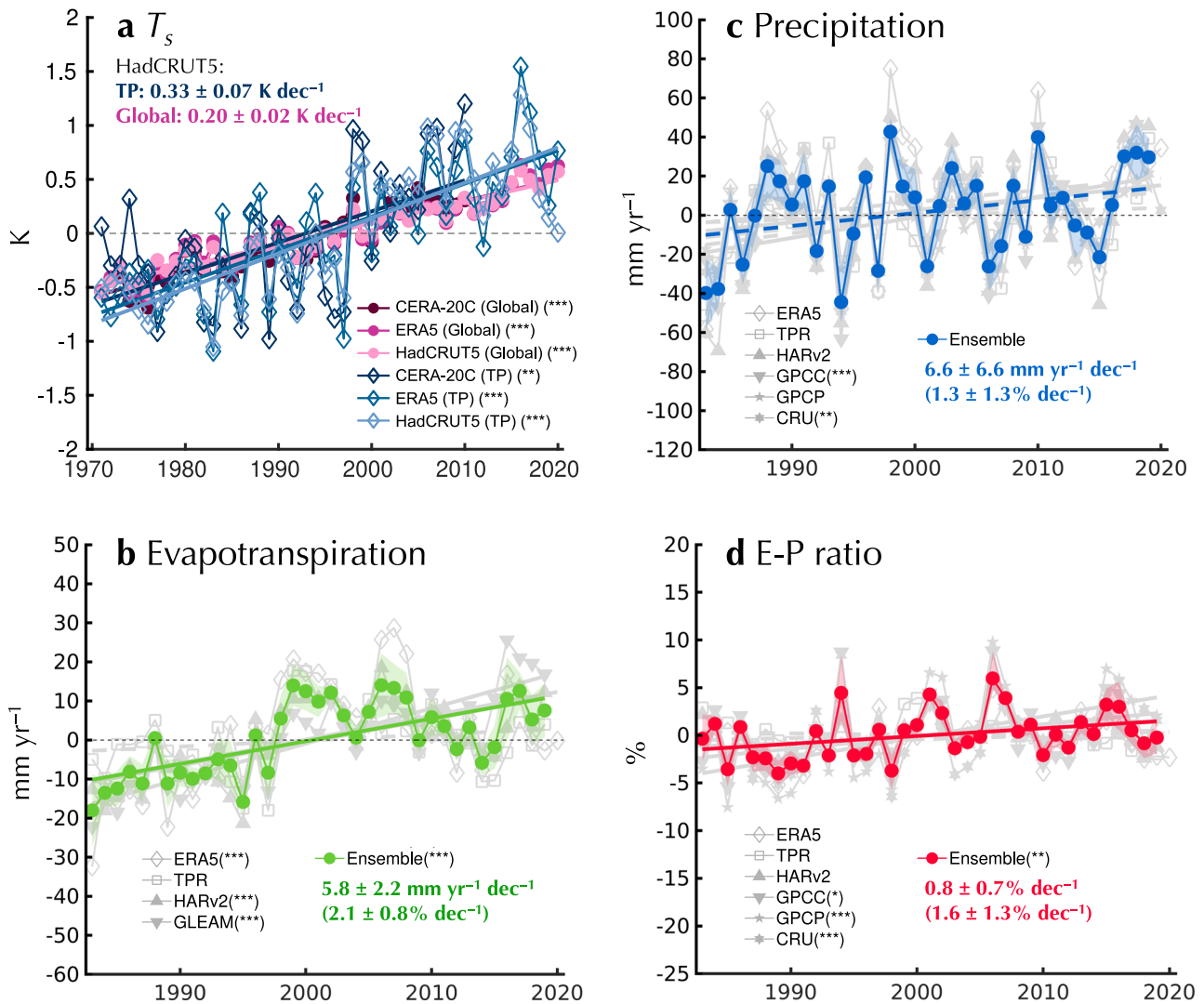
Fig. 2 | Long-term trends of temperature and water budgets in the TP. a Global near-surface air temperature (T_s) anomaly based on the CERA-20C, ERA5, and HadCRUT5 datasets (purple curves). Blue curves with hollow diamonds denote the T_s anomaly over the TP. The base period for the HadCRUT5 T_s anomaly is 1961–1990, while the base period for T_a for CERA-20C and ERA5 is 1981–2010 due to data availability. A solid line indicates a statistically significant trend at the 0.1 level (Mann–Kendall test), otherwise the trend lines are dashed. Various significance levels (*: 0.1, **: 0.05, ***: 0.01) are shown in the legend. **b** The TP evapotranspiration anomaly from various observational products and multi-product ensemble over the common period of 1983–2019. **c** Similar to (**b**), but for the TP precipitation. **d** Similar to (**b**), but for the TP evapotranspiration-precipitation (E-P) ratio. Shading in (**b**–**d**) denotes the inter-product uncertainty ranging from the 25th to the 75th percentile of the values. All values of the trends are tabulated in Supplementary Table 2.

(Fig. 1a). Meanwhile, the importance of the Indian Monsoon halves to 11.6 ± 1.4% as the hemispheric land-sea thermal contrast overturns[54]. For this reason, the hydrological regime along the entire Himalayas and the western TP turns westerly-dominated, accounting for 32.4% of the TP's surface area (see inset in Fig. 1a). As a side note, the role of the East Asian monsoon was likely overrated[3,12,29,42,55], given its contribution of less than 5% of the plateau-wide precipitation due to the western North Pacific subtropical high at work[56–59]. Nevertheless, grid cells in the far east of the TP are governed by the East Asian monsoon.

The inner TP precipitation strongly hinges on local land-atmosphere interactions. Terrestrial sources directly provide 85.2 ± 1.7% of the moisture supply to the Asian water tower, while direct contributions from the oceans account for approximately one-tenth or less (Fig. 1a). Since the oceans are the ultimate reservoirs for moisture over land, moisture must have undergone more than one precipitation-evaporation cycle before fueling precipitation high up the TP––a process known as cascading moisture recycling[51,60,61]. This process is supported by our grid-scale tracking outcome, showing that up to 62.6–74.3% of the TP's surface area is TP-

dominated––meaning that these areas receive the most moisture evaporated nonlocally from within the TP (Fig. 1a). The above results underscore the importance of cascading moisture recycling in maintaining the moderately strong precipitation recycling, illuminating that the TP's internal water cycle is considerably terrestrial and self-constrained by climatology.

The TP's growing dependence on precipitation recycling in present-day climate

The TP's climate sensitivity is characterized by rapid surface warming and notable shifts in its surface water budget and moisture recycling dynamics. Recent decades have witnessed the TP's surface warming at a rate of 0.33 ± 0.07 K dec^{-1} ($p < 0.01$), evidently faster than the global rate (0.20 ± 0.02 K dec^{-1}) by observations (Fig. 2a; Supplementary Table 1). Accompanying the rapid warming is a surge in evapotranspiration, increasing at 5.8 ± 2.2 mm yr^{-1} dec^{-1} ($p < 0.01$) based on the multi-product ensemble (see "Methods" section; Fig. 2b). In commensurate with a recent report[62], the TP's ensemble evapotranspiration exhibits a super CC-scaling at 8.7 ± 3.7% K^{-1} ($p < 0.01$) with respect to global mean surface temperature,

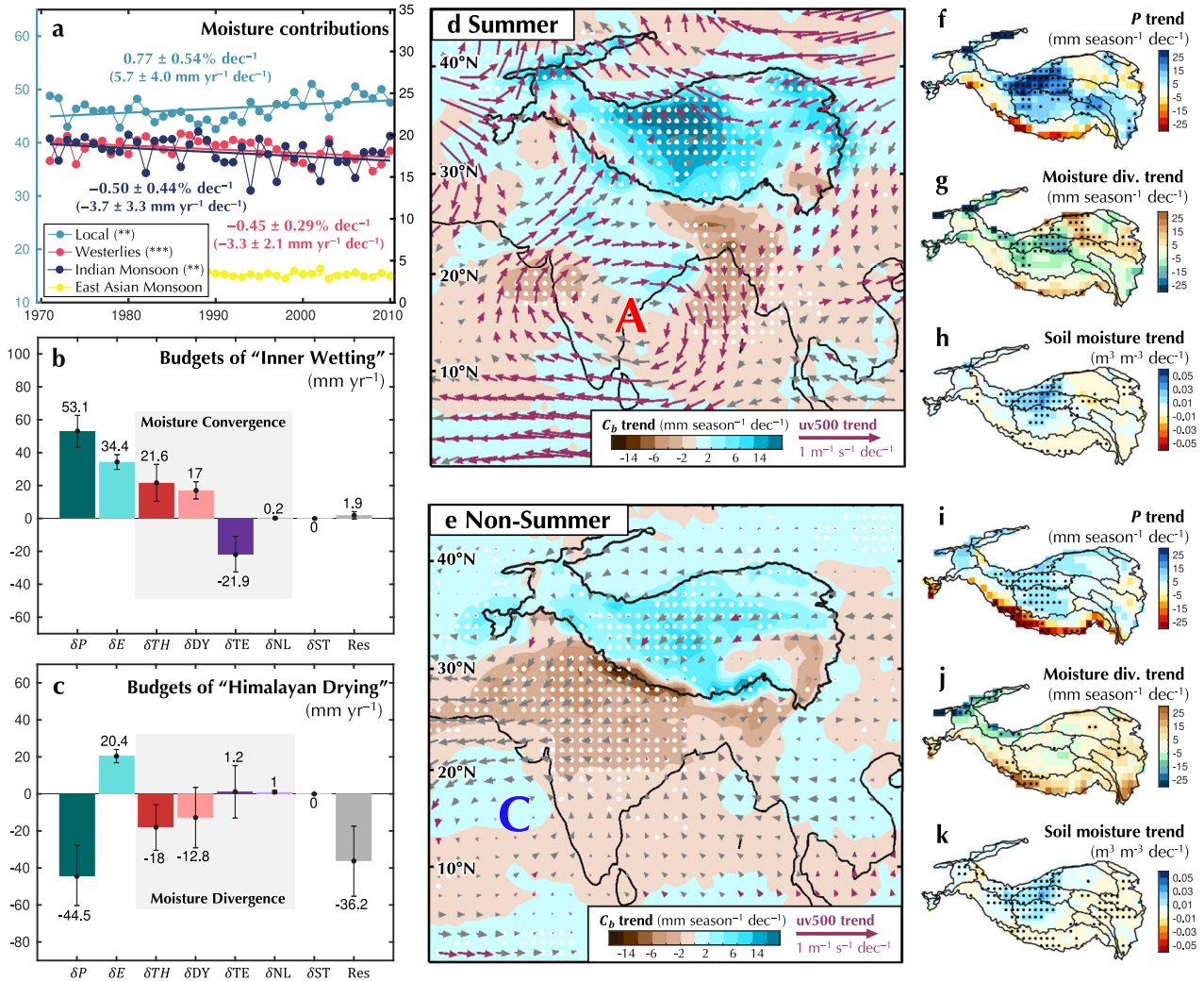**Fig. 3 | Physical processes in the TP's changing moisture recycling. a** Multi-curve plot showing changes in relative importance (unit: % dec^{-1}) of precipitation (local) recycling, westerlies, and the Indian and East Asian monsoon in the TP precipitation using the Lagrangian approach. The changes in the absolute moisture contribution (unit: mm yr^{-1} dec^{-1}) are shown based on the CERA-20C historical mean (1971–2010) annual total precipitation. The y-axis on the left side refers to precipitation recycling, while the right refers to the other variables. **b** Bar chart showing the decomposed moisture budgets that contribute to the inner wetting, based on the precipitation change (δP) in the southern and northern inner TP basins between the periods 1991–2010 and 1971–1990. Error bars denote the range from the 25th to the 75th percentiles of the bootstrapped values. **c** Similar to (**c**), but for the Himalayan Drying based on δP in the Yarlung Tsangpo basin. **d** Colors showing the long-term trends in C_b (unit: mm season^{-1} dec^{-1}) at the 0.1 significance level during summer. Vectors in purple represent the significant trends in the 500-hPa winds (unit: m s^{-1} dec^{-1}), otherwise are in grey. **e** Similar to (**e**), but for the non-summer season. The letter A denotes an anticyclonic circulation while the letter C denotes a cyclonic circulation. **f** The TP map displaying the trends in the seasonal precipitation (unit: mm season^{-1} dec^{-1}), **g** vertically integrated moisture divergence ($\frac{1}{g}\int_0^{P_s}\nabla\cdot q\mathbf{u}dp$, unit: mm season^{-1} dec^{-1}), and **h** the volumetric soil moisture content in the top layer (0–7 cm; unit: m^3 m^{-3} dec^{-1}) during summer. Stippling denotes significant trends at the 0.1 level (Mann–Kendall test). **i–k** Similar to (**g–i**), but for the non-summer season.

more than triple the global continental rate (2.8 ± 1.2% K^{-1}) (Supplementary Table 2). Likewise, the TP precipitation demonstrates a stronger scaling rate at 6.5 ± 6.0% K^{-1} than the global land rate (Supplementary Table 2). Given the faster growth in the ensemble evapotranspiration compared to precipitation by percentage change (Fig. 2b, c), the evapotranspiration-precipitation (E-P) ratio, which serves as a simple Eulerian indicator for maximal precipitation recycling ratio, consistently shows an upward trend of 0.8 ± 0.7% dec^{-1} (Fig. 2d). These findings entail a uniquely strong climate sensitivity of evapotranspiration and precipitation recycling in the Asian water tower.

To verify the hypothesis of precipitation recycling intensification in the TP, we conducted a four-decade-long Lagrangian tracking simulation. The simulation results unfold a significant increase in the TP's precipitation recycling ratio (i.e., the fractional contribution of local evapotranspiration to local precipitation through backward tracking[51,63]) at 0.77 ± 0.54% dec^{-1} ($p < 0.05$), which corresponds to an absolute rate of

5.7 ± 4.0 mm yr^{-1} dec^{-1} (Fig. 3a), in line with the upward trends in evapotranspiration and the E-P ratio (Fig. 2b, d). This tracking-based outcome highlights two important phenomena occurring in the Asian water tower: Firstly, its internal water cycle has been intensifying as a result of present-day warming. Secondly, its precipitation is increasingly influenced by local evapotranspiration. These changes are consistent with a marked increase in the moisture-source field plateau-wide (Fig. 3d, e). Warming acts to slow down the atmospheric overturning circulation as well[64–70]. Leveraging the Lagrangian method, we measure a significant decline in the year-round fractional contributions of the Indian monsoon at −0.50 ± 0.44% dec^{-1} (or −3.7 ± 3.3 mm yr^{-1} dec^{-1}) and the westerlies at −0.45 ± 0.29% dec^{-1} (or −3.3 ± 2.1 mm yr^{-1} dec^{-1}) (Fig. 3a). The above findings shed light on a gradual transition in dependence from nonlocal to local moisture recycling, underscoring a less-known concept that the Asian water tower is becoming increasingly self-constrained in response to climate change.

To further understand the physical processes in the moisture recycling changes, we consider the atmospheric water balance equation[71], which links precipitation to surface evapotranspiration and horizontal moisture fluxes. By means of moisture budget decomposition[65,72] (see "Methods" section), we show that the inner wetting––represented by the interdecadal precipitation change in the two inner TP basins––is primarily driven by a plateau-wide surge in evapotranspiration (δE) and, to a lesser extent, by enhanced moisture convergence. The latter includes both humidity-driven thermodynamic (δTH) effects and dynamic changes (δDY), which together outweigh the drying effect of transient eddies (δTE) (Fig. 3b). Albeit with a considerable residual term of the water budget in the Himalayas due to complex topography[65], this does not deny the significance of moisture divergence in negating the rising evapotranspiration and inducing the drying there (Fig. 3c).

Spatially, the decline in external moisture recycling is tied to the slowdown of the Indian summer monsoon, as evidenced by an increasing tendency of northeasterlies all over the Indian Ocean coupled with declining uptake of moisture from the ocean surface (Fig. 3d). In contrast, weakening westerlies across the TP are discernible from the easterly tendency of the 500-hPa winds during both summer and non-summer seasons (Fig. 3d, e). Column-integrated moisture convergence in the endorheic basins has been enhanced over the decades, connoting more moisture to converge from within the TP to initiate the inner wetting (Fig. 3f, g). Conversely, increasing moisture divergence along the Himalayas matches well with the increasing drought there (Fig. 3i, j). Considering the effect of soil moisture memory[73] and the TP's semi-arid climate[74], increasing soil moisture availability would positively feedback onto precipitation through moisture recycling and further maintain the inner wetting[75], and vice versa for the Himalayan Drying (Fig. 3h, k). In a nutshell, the TP's water cycle becomes increasingly self-constrained, driven by increased precipitation recycling due to surging evapotranspiration and enhanced moisture convergence from within and waning moisture supply from without.

A dual effect of the greenhouse gas (GHG) forcing

A conundrum remains: what fundamentally causes the TP's precipitation and moisture recycling changes? Here we examine single-forcing CMIP6 simulations from the Detection and Attribution Model Intercomparison Project (DAMIP)[40] (Supplementary Table 3). Most of the state-of-the-art CMIP6 climate models still struggled to reproduce the TP's contrasting precipitation change[23] (Supplementary Figs. 2, 3). As such, we carefully selected the best five models whose historical simulation satisfactorily reproduced such a pattern (Supplementary Table 4; see "Methods" section). Based on the best five models' ensemble (MME5), we corroborate a recent argument[23] that the observed inner wetting-Himalayan Drying was mainly attributed to anthropogenic aerosol forcing due to its cooling effect caused by reflection (Fig. 4a–d, i). However, such aerosol-induced drying will be temporary. As the GHG emission continues to soar while the cooling effect weakens as the result of mitigated anthropogenic aerosol emission (Supplementary Fig. 4), their combined effect will undo the drying and herald an overall wetting of the TP[23] (Fig. 4b, e–g).

Further, the dual effect of GHG forcing on the TP's changing environments will become increasingly paramount. Based on the historical single-GHG-forcing (hist-GHG) experiment, we discover that whilst the potent GHG warming boosts up the lower-level atmospheric moisture content on the TP (Fig. 4i), it also induces a top-heavy heating in the atmosphere[76]. This secondary effect of the GHG forcing is manifested in the enhanced alpine dry static stability (defined as $-\frac{T}{\theta}\frac{\partial\theta}{\partial p}$ at 400 hPa). It shows that the GHG-induced top-heavy heating acts to stabilize the mid-to-upper troposphere (Fig. 4p), triggering a tendency of anticyclonic circulation over the TP (Fig. 4w). Accompanied by the anticyclone tendency is a northerly wind tendency that attenuates the southerly monsoons across the Himalayas. This finding underlines the role of GHG forcing in weakening the Indian monsoon-associated moisture transport to the Asian water tower, echoing our foregoing results by the Lagrangian method (Fig. 3a). This same GHG effect on atmospheric stabilization and monsoon slowdown is

consistently projected in all the three future scenarios (Fig. 4s–u, z–ab), especially when the aerosol effect weakens (Supplementary Fig. 4). The overall effects of anthropogenic forcings in both summer and non-summer periods resemble that of the annual pattern (Supplementary Figs. 5 and 6). Taken together, the dual effect of GHG forcing will continue to heighten the future sensitivity of the TP to precipitation recycling while diminishing dependence on external moisture advection, rendering the hydrological cycle more dependent on local land-atmosphere interaction.

The increasing role of TP evapotranspiration in future scenarios

The observed precipitation recycling intensification over the TP is just the prelude to its forthcoming trend. The best five climate models suggest that the TP evapotranspiration exhibits a robust upward trend in a warming climate, particularly in the high-end scenario with a rate of 15 ± 0.4 mm yr^{-1} dec^{-1} (Fig. 5a). Further, its relative growth ($2.9 \pm 0.07\%$ dec^{-1}) is projected to be effectively faster than that of precipitation ($2.6 \pm 0.08\%$ dec^{-1}) on the TP under the SSP5-8.5 run, as likewise seen in the SSP3-7.0 and SSP2-4.5 runs (Fig. 5a, b). Examining the projected E-P ratio reaffirms the faster growth of evapotranspiration than precipitation across all five best models (Fig. 5c). The clear upward trend in the future E-P ratio is in tandem with the present-day trend by observations (Figs. 2d and 5c). Further seasonal analysis reveals that the future surge in the E-P ratio comes primarily from the non-summer period when the rise in precipitation is apparently slower than that of evapotranspiration (Supplementary Fig. 7), which is likely due to the presence of increased soil moisture content by thawing snows.

The uniqueness of the TP's pronounced climate sensitivity is consistently projected in future scenarios. Due to the TP's more rapid warming in future scenarios (Supplementary Fig. 8), both evapotranspiration and precipitation in the TP ramp up two to three folds faster than the global rates (Fig. 5d). Again, the models project an effectively faster rate of change of the TP's evapotranspiration with respect to warming ($5.1 \pm 0.07\%$ K^{-1}) than that of precipitation ($4.1 \pm 0.17\%$ K^{-1}) in the SSP3-7.0 run (Fig. 5d), as consistently found in the other two scenarios (Supplementary Fig. 9). In harmony with the stabilizing effect of GHGs on the atmosphere and the divergence trend over the plateau, the average 500-hPa meridional wind velocity across the southern TP is projected to decrease significantly at a rate of $-10 \pm 1.1\%$ dec^{-1} in percentage under the SSP5-8.5 pathway (Fig. 5e). Conversely, the northward moisture transport across the southern TP is expected to increase steadily at a slower rate ($2.7 \pm 0.2\%$ dec^{-1}) throughout the 21st century. The ever-growing northward moisture transport evidently results from the enhanced specific humidity (Fig. 4n) that offsets the future weakening of the southerly monsoon flows, which explains the increase in the future TP precipitation. Given the foregoing findings alongside the high correlation coefficient (0.72, $p < 0.01$) between evapotranspiration and precipitation recycling ratio derived from the Lagrangian method (Fig. 5f), we conclude that the TP's water cycle will continue to be more sensitive to evapotranspiration and vulnerable to local land-atmosphere interaction in a warmer world. This pivotal conclusion holds important implications for water tower management, regional climate modeling, and decision-making, which will be further discussed in the next section.

Discussion

In concert with a recent work by Jiang et al.[23] on the impact of reduced anthropogenic aerosol emission and the moistening effect of the GHG forcing in the Asian water tower's recent hydroclimatic change, here we bring further attention to the lesser-known dual effect of GHG forcing. On the one hand, the GHG forcing contributes to continuous inner wetting through warming, enhanced evapotranspiration, and local recycling intensification. On the other hand, it causes top-heavy heating[76] that tends to stabilize the atmosphere and slows down southwesterly monsoons across the Himalayas, verified by both the single-forcing hist-GHG experiment and the SSP2-4.5 and SSP5-8.5 scenarios shown herein. The GHG-induced anticyclonic circulation (divergence) tendency over the future TP
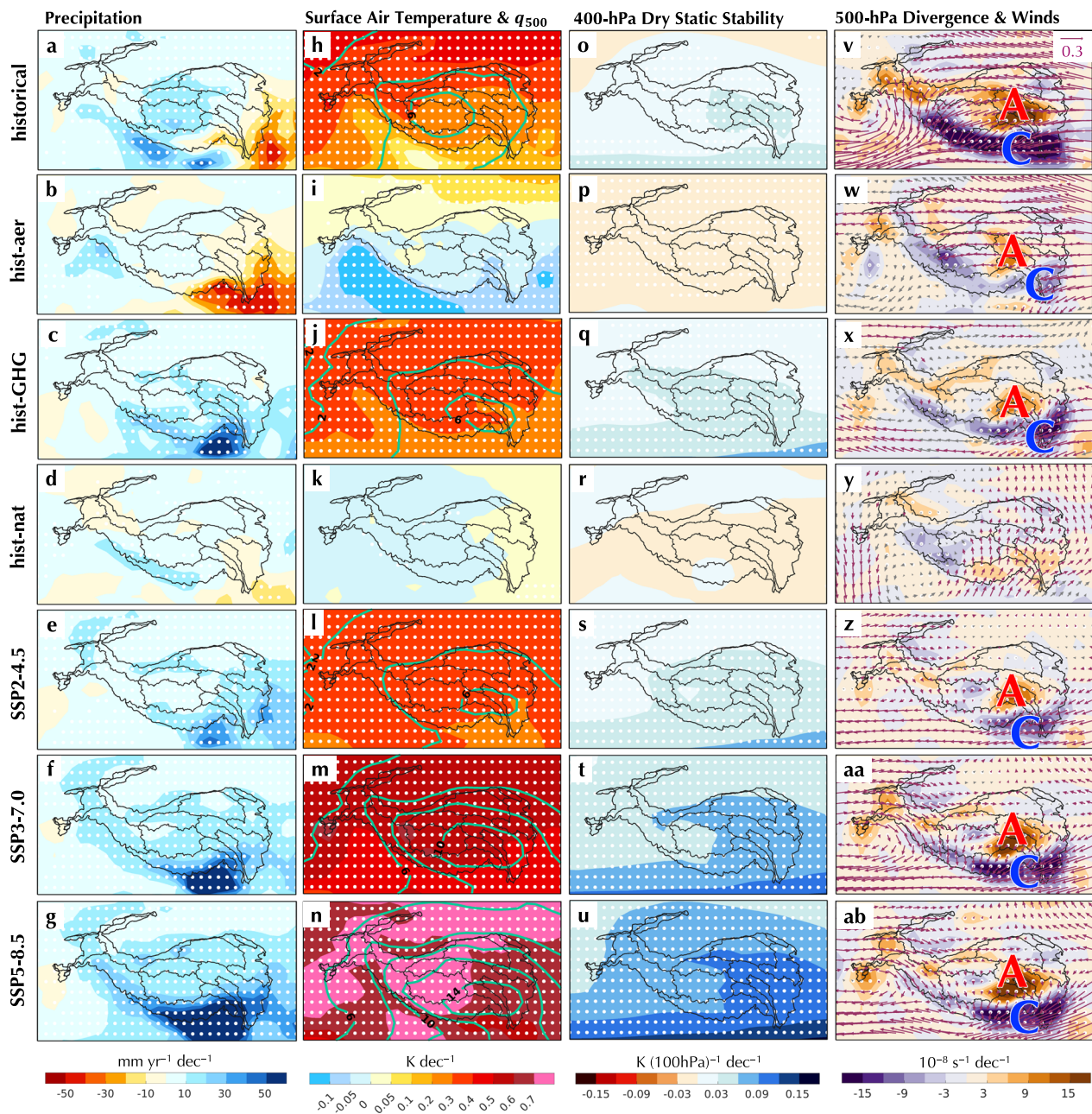
Fig. 4 | Long-term trends in the meteorological conditions of high mountain Asia based on CMIP6 models. Column 1 showing trends in precipitation (P, unit: mm yr^{-1} dec^{-1}) for **a** historical, **b** hist-aer, **c** hist-GHG, **d** hist-nat, **e** SSP2-4.5, **f** SSP3-7.0, and **g** SSP5-8.5 simulations based on MME5. The periods of the four historical simulations and the two future projections are 1971–2014 and 2015–2100, respectively. Columns 2–4 are similar to Column 1, but for the trends in (**h–n**), surface air temperature (shading, unit: K dec^{-1}), and the 500-hPa specific humidity, q_{500} (contour, unit: 10^{-1} kg kg^{-1} dec^{-1}) with green/brown contours indicating positive/ negative values, **o–u** the 400-hPa dry static stability (unit: K (100 hPa)$^{-1}$ dec^{-1}), and **v–ab** the 500-hPa divergence (unit: 10^{-8} s^{-1} dec^{-1}) and winds (unit: m s^{-1} dec^{-1}). Letter A denotes an anticyclonic circulation tendency while letter C denotes a cyclonic circulation tendency. Contours shown in (**h–n**) are statistically significant at the 0.1 level (Mann–Kendall test) while sharding and vector variables are statistically significant only when they are denoted by stippling and purple vectors, respectively.

foreshadows a reduction in the number or strength of the TP vortices[77] under warming, agreeing well with recent observations[78]. Zhang et al.[79] concluded that the warming-induced terrestrial water storage deficit in the TP was influenced more prominently by surface water budget deficit from the North Atlantic Ocean than from the Indian Ocean and local moisture sources using the same 3D Lagrangian model but a different moisture-source diagnostic from this study. While their finding is commensurate with the declining westerly-associated contribution found in this work, we further disentangle the countering effect of the precipitation recycling intensification against the attenuating water vapor supply from the mid-latitude

westerlies and Indian summer monsoon, which elucidates the TP's inner wetting. In virtue of water vapor transport decomposition along the TP's four boundaries, Wang et al.[80] affirmed a pronounced decrease in water vapor export from the eastern boundary due to anthropogenic aerosol forcing that modifies meridional temperature gradient[23] and thereby incites an anomalous Rossby wave train. Their outcome harmonizes well with the weakening mid-latitude westerlies and enhanced precipitation recycling over the TP based on our Lagrangian tracking method.

Distinguished from the previous endeavors, this work offers compelling evidence from a 40-year 3D Lagrangian tracking simulation and water
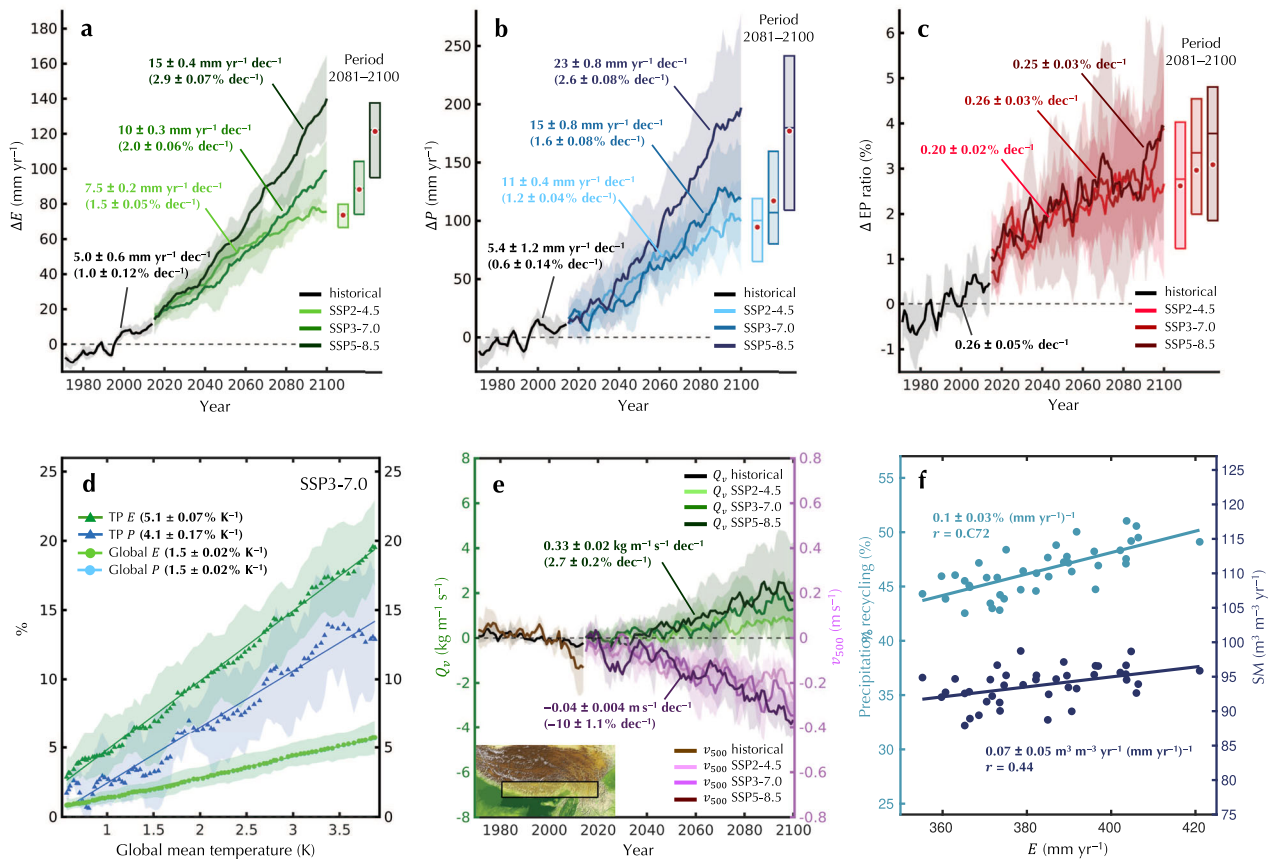
Fig. 5 | The growing importance of evapotranspiration in the TP's future water cycle. a The projected change in the TP evapotranspiration (unit: mm yr^{-1} dec^{-1}) in the SSP2-4.5, SSP3-7.0, and SSP5-8.5 till the year 2100 with respect to the historical mean (1971–2014) based on the MME5. Shading denotes the inter-model spread ranges from the 25th to the 75th percentile. The relative trends are shown in parentheses. Boxplots on the right show the distribution in the far-future period of 2081–2100, with bars denoting the 25th, 50th, and 75th percentiles and a red dot indicating the mean. **b, c** Similar to (**a**), but for the projected TP precipitation and the E-P ratio, respectively. **d** The projected TP and global evapotranspiration and precipitation scaling with respect to global mean surface temperature (unit: % K^{-1}) over the period of 2015–2100 in the SSP3-7.0 run. **e** Similar to (**a**), but for the projected 500-hPa meridional wind (v_{500}) and the meridional vertically integrated moisture transport (Q_v) averaged over the southern TP (as outlined in the inset). For simplicity, only the trends in the SSP5-8.5 run are shown. A 5-year running mean is applied to the time series in (**a**–**e**). **f** Scatter plot of the Lagrangian tracking-derived precipitation recycling ratio (unit: %) and the volumetric soil moisture (SM) content in the top layer (0–7 cm) (unit: m^3 m^{-3}) against the TP evapotranspiration (unit: mm yr^{-1}). The solid line represents the regression line alongside the slope and the Pearson correlation coefficients. All trends shown in (**a**–**f**) are statistically significant at the 0.01 level (Mann–Kendall test).

budget analysis to support the idea that the TP's recent precipitation changes are driven by enhanced precipitation recycling and moisture convergence that offset the steady decline in the Indian monsoon- and westerly-associated moisture transport. This outcome corroborates fragmented findings from the existing literature[22,29,32,35]. Most importantly, we discover that the TP's hydrological cycle becomes increasingly self-constrained––that is, more dependent on its local recycling and less on external moisture supply. This is evidenced by the prominently faster growth of evapotranspiration than precipitation on the TP in percentage change with respect to warming in both present and future climates. The expected enhancement of the TP's precipitation recycling ratio under a warmer climate drawn from the CMIP6 multi-model ensemble agrees with a recent modeling study using a higher-resolution regional climate model (Weather Research and Forecasting, WRF) simulation forced by a global climate model[81]. Additionally, we show a different mechanism by backward Lagrangian tracking that the moisture transport in the southern TP precipitation is primarily in the form of upslope flows (Supplementary Fig. 10), challenging the previous claim regarding the dominant role of up-and-over transport in the region[82].

However, the limitations of this study are worth noting[23]. While the MME5 is based on the top-performing five CMIP6 models in reproducing the observed precipitation change on the TP, their simulations are not

flawless. This is shown by the notable inter-model spread in the simulated water budget on the TP (Fig. 5a–d). With approximately 70 models participating in CMIP6, only about one-fifth of the models contributed to the tier-1 DAMIP experiments. More models to join DAMIP may help reduce further the cross-model uncertainties. Resolving the inherent deficiency in contemporary climate models[83] to realistically simulate land-atmosphere feedback is also essential. A comprehensive review of the past 16 studies[25–38,46] (Table 1) reveals a large uncertainty range in the estimates of the TP's precipitation recycling ratio during boreal summer (~10–80%) and throughout the year (~10–63.2%). Dependent on the methodology used, studies using Eulerian models[29–37] generally reported a relatively lower precipitation recycling ratio (~10–20%), since these simple models ignore the cascading moisture effect in the real world that the FLEXPART-WaterSip approach considers[45,46,84,85]. Further, 2D models fail to resolve the full vertical profile of the atmosphere and moisture flows across the complex topography[86] and are subject to well-mixed conditions that are seldom met in reality[87]. In contrast, isotopic studies[25–27] and budget analysis[28] reported a higher precipitation recycling ratio of 30–80% for the summer precipitation and 53.2–63.2% for annual precipitation in the TP (Table 1). However, it is important to realize that isotopic studies may be subject to sampling issues while budget analysis may depend on data quality and method. Hence, our Lagrangian estimates (52.2% for summer precipitation and 46.5% for

annual precipitation) that fall between the two groups of estimates could be considered reasonable. It is noteworthy that the precipitation recycling ratio is scale- and shape-dependent[63,88]. Even worse, the boundaries of the TP were not defined consistently in the literature[3,28,29,31,38,46]. This explains the exceptionally smaller estimates of the precipitation recycling ratio reported by Sun and Wang[46], for their analysis was based on a tiny box region in the northeast TP. However, the 3D Lagrangian tracking method has its deficiencies as well. The derived trajectories could still suffer from uncertainties due to convection, turbulence, rainwater evaporation, and numerical diffusion[45,51]. Future intercomparison studies are needed to reconcile estimates and hopefully reduce uncertainties regarding the TP's moisture recycling ratios.

Finally, what are the key implications given the foreglimpse of the TP's increasingly vulnerable water cycle under climate change? Firstly, it foreshadows a growing role of land-atmosphere interaction in the region's water and energy cycle. Soil moisture is positively correlated (0.44, $p < 0.01$) with evapotranspiration on the TP (Fig. 5f), suggesting that the TP is essentially a water-limiting regime where soil moisture controls evapotranspiration[73]. Due to human-induced warming, enhanced precipitation and rapid melting of alpine glaciers result in increased inflow of water into the soils and lakes[10,12,13], leading to accelerated evapotranspiration[62] that feeds back to a stronger precipitation recycling process. Vegetation migration will play a part in the TP's future hydroclimate as well. An observational study[19] suggested an overall greening on the TP in the past decades, manifested in increasingly more steppe (semi-desert) replaced with meadow (grassland). This observation could result from faster wetting and precipitation recycling intensification in the semi-desert environment than elsewhere on the TP based on our tracking results (Supplementary Fig. 11). Secondly, with the waning percentage of external moisture supply and stronger precipitation recycling, runaway droughts could occur during dry years when the replenishment of terrestrial water storage is slower than depletion by evapotranspiration and surface runoff. This will exacerbate water scarcity, causing ecological imbalances and increased competition over limited freshwater resources. Other hazards, such as land degradation due to alpine permafrost collapse[15,17] and glacial lake outburst floods[89,90], will be amplified as more locally evaporated water vapors fall as warmer raindrops in the future. Thirdly, the altered water cycle can have broader and cascading effects on weather patterns and climate Earth-wide[91], rendering the TP a potential but less-understood tipping point in the climate system[92,93]. This calls for more extensive gauge observations and field measurements to aid climate models in better simulating the complex interplay between the atmosphere, cryosphere, hydrology, and alpine plant physiological response in the region for decision-making. Lastly, the TP's increasingly vulnerable water cycle under climate change requires careful attention and effective, far-sighted water tower management among different Asian sectors and countries[5] to mitigate the potential risks and ensure sustainable and equitable water use and sharing, as well as to safeguard food security, livelihoods, and long-term economic development in a changing climate.

Methods
Observational datasets and reanalysis
Pressure-level and surface environmental fields were retrieved from the 3-hourly, $1° \times 1°$ CERA-20C reanalysis product[94] for diagnosis, while the terrain-following, model-level data were adopted to force the Lagrangian model. We used the hydrologically well-defined, level-3 catchment boundaries from the hydrologic data and maps of the shuttle elevation derivatives at multiple scales (HydroSHEDS) database[95] to benchmark the estimates of moisture recycling ratios. The shape files of the boundaries of the TP (outlined by an altitude of 3000 m) and its upstream and downstream catchments are accessible from our data availability statement. Additional sources of reanalysis and observational data were adopted to evaluate the bias in CERA-20C moisture budgets. Reanalysis products included the fifth generation European Centre for Medium-Range Weather Forecast (ECMWF) reanalysis (ERA5)[96], high Asia refined analysis version 2 (HARv2)[97], and the TP reanalysis (TPR)[98,99]. HARv2 is derived from the

dynamical downscaling of the WRF model, forced by ERA5 reanalysis and Japanese 55-year reanalysis (JRA-55) snow depth data[97]. Similarly, the TPR is a dynamically downscaled product using the ERA5-forced WRF simulation at 9-km resolution and a different nudging technique, reproducing precipitation more realistically than HARv2[98,99]. Long-term observation-based products were adopted in the bias evaluation of CERA-20C, including the Global Precipitation Climatology Project (GPCP)[100], Global Precipitation Climatology Centre (GPCC)[101], precipitation from the Climatic Research Unit (CRU)[102], evapotranspiration from GLEAM[103,104], and near-surface air temperature from HadCRUT5[105]. Other satellite-based precipitation products, such as IMERG[106] and CMOPRH[107], were excluded from our analysis owing to their limited temporal coverage (~20 years) and sub-par performance in detecting shallow and warm orographic precipitation events[98,108]. Details of the datasets used herein are summarized in Supplementary Table 1.

Multi-product ensemble
Given the scarcity of ground-based observations on the TP[3,109], it is necessary to construct a multi-product ensemble to understand the status quo of the alpine atmospheric water cycle. The ensemble-mean evapotranspiration was constructed using a satellite-based GLEAM product, ERA5 reanalysis, and two model-based products (HARv2 and TPR) over a common period of 1983–2019 (Fig. 2b). Likewise, the ensemble-mean precipitation is computed by averaging the three long-term observational products (i.e., CRU, GPCC, and GPCP) and the three reanalysis or model-based products (i.e., ERA5, HARv2, and TPR) (Fig. 2c). As a simple indicator of precipitation recycling ratio, the observational E-P ratios were computed by dividing GLEAM evapotranspiration by the observational precipitation products (CRU, GPCC, and GPCP), while the reanalysis/model-based E-P ratios were computed based on the products' own evapotranspiration and precipitation fields (Fig. 2d). The two regional, TP-centered HARv2 and TPR datasets were excluded from the multi-product ensemble when computing trends regarding the global land region (Supplementary Table 2).

Bias evaluation of CERA-20C reanalysis
The multi-product ensemble (whose fusion excluded CERA-20C) served as a benchmark to evaluate the quality of CERA-20C used to force the FLEXPART model. Despite a wet bias of CERA-20C precipitation (and similarly for ERA5 precipitation), it exhibits a high PCC (>0.8) with the ensemble-mean precipitation for both the Asia-Pacific domain and the TP alone (Supplementary Fig. 12a, b, h). Notably, the PCC between CERA-20C and observational products (e.g., CRU, GPCC, and GPCP) reached 0.9 individually (Supplementary Fig. 12c–e), while CERA-20C generally showed the lowest PCC and highest RMSE with downscaled products (Supplementary Fig. 12f, g). In terms of long-term trends, CERA-20C satisfactorily reproduced the north-south contrast in precipitation trend over the TP and exhibited the highest PCC with the ensemble-mean product among all others (Supplementary Fig. 13). Likewise, the spatial pattern and long-term trend of the mean CERA-20C evapotranspiration were similar to those of the ensemble-mean product (Supplementary Figs. 14, 15). The foregoing evaluation justifies the use of CERA-20C in forcing the FLEXPART model.

CMIP6 data, experiments, and model evaluation
The CMIP6 DAMIP[40,110] provides state-of-the-art climate change detection and attribution on how the Earth's climate system responds to single anthropogenic and natural forcings. The tier-1 DAMIP experiments include historical (with all natural and anthropogenic forcings), hist-GHG (with well-mixed greenhouse gas forcing only), hist-aer (with anthropogenic forcing only), and hist-nat (with solar, volcanic, and stratospheric aerosol forcings only) experiments[40]. Here we assessed 12 CMIP6 models participating in DAMIP (Supplementary Table 3). These models provided complete simulation results for the tier-1 DAMIP and the ScenarioMIP experiments, including the mitigated scenario with a radiative forcing at 4.5 W m^{-2} by the year 2100 (SSP2-4.5), the medium-to-high-end scenario

with high societal vulnerability and a radiative forcing at 7.0 W m^{-2} by the year 2100 (SSP3-7.0), and the unmitigated, high-end scenario with a radiative forcing at 8.5 W m^{-2} by the year 2100 (SSP5-8.5)[41]. While none of the models can perfectly reproduce the precipitation climatology and trend (Supplementary Figs. 2, 3), the best five (CNRM-CM6-1, MRI-ESM2-0, ACCESS-ESM1-5, ACCESS-CM2, and GFDL-ESM4) were selected based on their fine performance in simulating the observed inner wetting-Himalayan drying pattern (Supplementary Table 4).

Lagrangian tracking simulation

We performed a four-decade-long (1971−2010) simulation of 3D Lagrangian tracking using the FLEXible PARTicle dispersion (FLEXPART) model version 10.4[44,51,111]. Compared to 2D models, 3D models typically offer an improved accuracy of the air parcel trajectory[87,112,113]. FLEXPART uses an offline tracking technique—that is, the model is driven (and therefore constrained) by reanalysis data without the need to numerically solve the coupled prognostic equations. For this reason, offline tracking models are computationally more efficient than numerical weather simulations using online water-tagging methods[114,115]. The model was driven by CERA-20C reanalysis that offers up to 91 terrain-following model levels, which allows more realistic simulations of the motion of air parcels over the complex topography of the TP[111]. The model ran in a domain-filling mode, in which the global atmosphere was homogeneously divided into 5 million air parcels with equal masses. The model internally simulated the 3D motion of the parcels every 15 min and output the results every three hours. Interested readers are referred to Cheng and Lu[51] for details of the moisture tracking simulation.

Optimized Lagrangian moisture-source diagnostic

Precipitation variability links to changes in local and nonlocal moisture recycling[51,63,116]. Local moisture recycling (or precipitation recycling) refers to a process in which precipitation is contributed by moisture evaporated locally[117,118]. Nonlocal moisture recycling involves moisture contributed from an external source through wind advection[60,119,120]. To quantify moisture recycling, here we adopt a Lagrangian diagnostic called WaterSip[45,61]. The diagnostic uses the moisture trajectories from the FLEXPART simulation to compute the relative contributions of the upwind water uptakes to the TP precipitation. The WaterSip diagnostic takes into account the cascading effect of the loss of moisture en route that would discount the contribution of earlier moisture uptake to the target precipitation event.

One crucial step of the WaterSip diagnostic is to determine precipitating air parcels, from which the accumulated water loss ought to be comparable with the surface precipitation. A key parameter here is the Lagrangian-estimated precipitation P_{LA}[51], whose value at time t is calculated as:

$$P_{LA}(x, y, t) \approx \frac{1}{A(x, y)} \sum_{k=1}^{K} m_k \Delta q_k [\mathbf{x}'_k(0)], \tag{1}$$

$$\text{for } \Delta q_k [\mathbf{x}'_k(0)] < \Delta q_c \text{ and } RH_k [\mathbf{x}'_k(-3hr)] > RH_c(x, y),$$

where $\mathbf{x}'(\tau)$ is the 3D location $[x'(\tau), y'(\tau), z'(\tau)]$ of the parcel, τ is the backtracking time, $\Delta q_k [\mathbf{x}'_k(0)]$ is the change in the air parcel k's specific humidity at the initial position ($\tau = 0$) at time t, A is the grid area, K is the total number of parcels within the air column at the grid cell (x, y), m_k is the mass of the parcel k, and Δq_c (taken as -0.1 g kg^{-1} (3 h)$^{-1}$) and RH_c are the thresholds of specific humidity and relative humidity (RH) upon precipitation, respectively. It is worth mentioning that Eq. (1) assumes a negligible evaporation rate of the moisture of the parcel during rainout[121]. When tracking air parcels, errors may arise and accumulate over time due to numerical diffusion and chaos, leading to unrealistic trajectories. To alleviate this issue, we implemented an optimal-tracking mode[51] to ensure that the tracking is terminated if over 99% of the source of precipitation has been traced or when the tracking period exceeds

20 days. Interested readers are referred to Sodemann et al.[45] for the detailed algorithm of the diagnostic.

As P_{LA} is primarily controlled by RH$_c$[51,85], we devised a spatially and seasonally varying scheme for RH$_c$ to minimize the biases of P_{LA} from the surface precipitation P (Supplementary Fig. 16). Compared with the results based on a fixed RH$_c$ of 85%, the scheme produced much-improved precipitation through lowering RH$_c$ in the TP (Supplementary Fig. 17a−c), where fast recycling of precipitation frequently occurs owing to mechanical lifting in the mountainous topography[85,122]. Further, the RH$_c$ scheme minimized the biases caused by seasonal variations in atmospheric circulations, boundary layer mixing, and land surface conditions to an extent where the Pearson pattern correlation coefficient (PCC) remained >0.9 with a root-mean-square-error (RMSE) <1 mm day^{-1} (Supplementary Fig. 17d−g). All of the above lends credibility to the result of the WaterSip diagnostic presented hereafter.

Given the moisture recycling ratio ρ estimated by the WaterSip diagnostic, the backward moisture-source field C_b (unit: mm (3 h)$^{-1}$)––also known as precipitation footprints[50,51]–at time t is computed by:

$$C_b(x, y, t) = \frac{1}{A(x, y)} \sum_{k=1}^{K} \sum_{\substack{\tau = -\tau_N, \\ \mathbf{x}'_k(\tau) \in (x, y)}}^{0} m_k \rho_k [\mathbf{x}'_k(\tau)] \Delta q_k [\mathbf{x}'_k(0)], \tag{2}$$

where the inner summation amasses all the relative contributions of the water uptakes (i.e., effective water uptakes) along the trajectory from the total backtracking time (τ_N) to the starting time ($\tau = 0$) at time t in the column (x, y), and the other parameters follow the same notation as in Eq. (1). Aggregating the sub-daily C_b gives daily values in units of mm day^{-1}.

Circulation regime classification

To evaluate the relative importance of the monsoons and westerlies in the TP precipitation in a systematic and objective manner, it is imperative to determine their spatial regimes in the first place. Here we propose a compact monsoon-westerly index (MWI), defined as:

$$MWI = \mathbf{u}_{300} \cdot \mathbf{u}_{850}, \tag{3}$$

where $\mathbf{u}_{300}$ and $\mathbf{u}_{850}$ refer to the horizontal winds at 300 and 850 hPa, respectively, and ($\cdot$) denotes the dot product operator. A significantly negative MWI at the 0.01 level (Student's t-test) indicates an overturning regime, in which the upper- and lower-level winds blow in almost reversed directions in a baroclinic atmosphere. Conversely, a significantly positive value denotes a westerly/easterly regime wherein the wind direction is consistent at both lower and upper levels in a barotropic atmosphere. The WMI magnitudes and the corresponding confidence interval at the 0.01 level are shown in Supplementary Fig. 18 for the readers' reference. The compact WMI can effectively capture the monsoon regimes globally, such as the North American monsoon[123,124], South American monsoon[125,126], Australian monsoon[127,128], Indian monsoon[54,56], and the East Asian monsoon domains[56,57,129] (Supplementary Fig. 19a).

Of relevance to the TP precipitation, the Indian monsoon and East Asian monsoon regimes are defined as the grid cells of the overturning regime that fall within the pan-Indian monsoon and pan-East Asian monsoon domains, respectively (Supplementary Fig. 19a). The overturning regimes outside the above two domains are regarded as other monsoons for simplicity. We define the Northern Hemisphere mid-latitude and Arctic westerly regimes within 15−60 °N and 60−90 °N, respectively. The Southern Hemisphere westerly regime is defined as the westerly regime poleward of 15 °S. The easterly regime is defined within 30° of the equator, except in North India where the easterly regime is grouped into the Indian monsoon regime during summer, for it is, in fact, part of the Indian summer monsoon trough system[54]. Notice that the MWI developed in this study is based on both upper and lower levels. Thus, the derived circulation regime classification must differ from those based on a single level. However, they

are generally consistent. For example, the westerly regime in the northeast part of East Asia (Supplementary Fig. 19b) is consistent with the core location of the westerly jet stream[53], also known as the exit region of the jet[130]. Over the annual cycle, the westerly regime captures the seasonal migration of westerly jets straddling the TP[53,131]. To account for the seasonal variations in the regimes, a regime's annual total moisture contribution to the TP is calculated by taking the area-weighted sum of the TP's seasonal total precipitation multiplied by its corresponding seasonal importance, and similarly for computing the non-JJA contribution.

Moisture budget decomposition

Moisture budget decomposition is useful in disentangling various physical processes pertinent to the precipitation change. The decomposition originates from the vertically integrated water balance equation[71,72]:

$$P - E = -\frac{1}{\rho_w g} \int_0^{p_s} \frac{\partial q}{\partial t} + \nabla \cdot (\mathbf{u}q) + \frac{\partial}{\partial p}(\omega q)\, dp, \quad (4)$$

where ρ_w is the density of water (i.e., 997 kg m^{-3}), g is the gravitational constant (i.e., 9.81 m s^{-2}), q is the specific humidity (unit: kg kg^{-1}), p is the pressure (unit: Pa), p_s is the surface pressure (unit: Pa), $\mathbf{u} \equiv (u, v)$ is the horizontal wind velocity (unit: m s^{-1}), and ω is the pressure velocity (unit: Pa s^{-1}).

Based on Eq. (4), the change in precipitation between two different periods (δP) can be decomposed into the contributions owing to evapotranspiration (δE), thermodynamic (δTH) and dynamic effects (δDY), and transient eddies (δTE), nonlinear (δNL), and moisture storage (δST) terms[65,72]. Namely,

$$\delta P = \delta E + \delta TH + \delta DY + \delta TE + \delta NL + \delta ST + Res, \quad (5)$$

where

$$\delta TH = -\frac{1}{\rho_w g} \int_0^{p_s} \nabla \cdot (\delta \bar{q} \bar{\mathbf{u}}_1)\, dp, \quad (6)$$

$$\delta DY = -\frac{1}{\rho_w g} \int_0^{p_s} \nabla \cdot (\bar{q}_1 \delta \bar{\mathbf{u}})\, dp, \quad (7)$$

$$\delta TE = -\frac{1}{\rho_w g} \int_0^{p_s} \nabla \cdot \delta (\overline{q'\mathbf{u}'})\, dp, \quad (8)$$

$$\delta NL = -\frac{1}{\rho_w g} \int_0^{p_s} \nabla \cdot (\delta \bar{\mathbf{u}} \delta \bar{q})\, dp, \quad (9)$$

$$\delta ST = -\frac{1}{\rho_w g} \int_0^{p_s} \delta \left(\overline{\frac{\partial q}{\partial t}}\right) dp, \quad (10)$$

$$\text{and } \delta(\cdot) = (\cdot)_2 - (\cdot)_1 \quad (11)$$

$\delta(\cdot)$ denotes the difference in a quantity between periods 2 and 1 (denoted by subscripts 1 and 2), and they were chosen to be 1991–2010 and 1971–1990, respectively. Overbars denote temporal means (e.g., over a season) and primes are the departures from the means (i.e., Reynolds averaging). Res denotes the residual term, and ∇ denotes the divergence operator. The vertical integration was taken from p_s to 10 hPa. Since near-surface specific humidity is absent in both CERA-20C and ERA5 reanalysis products, the surface term is omitted in Eq. (5) and incorporated into the residual term. It should be noted that while Eq. (6) is termed a thermodynamic effect[65,72], it is a humidity effect in a strict sense, for the thermodynamic effect is determined by both humidity and temperature.

Statistical analysis

The two-sided non-parametric Mann–Kendall test was adopted to assess the statistical significance of long-term trends in the variables. The two-sided Student's t-test with a null hypothesis of zero was used to determine statistically significant MWI. The uncertainties in the tracking-based ratio contributions are based on interannual variability (±one standard deviation). The uncertainties in the regression analysis referred to the 95% confidence level for the regression coefficient based on standard error. The lower and upper error bars of the decomposed moisture budget refer to the 25th and 75th percentile of the values from 10,000 bootstrap samples, respectively. The CMIP6 inter-model spread ranges from the 25th to 75th percentile of the values.

Data availability

Code availability

References

1. Xu, X., Lu, C., Shi, X. & Gao, S. World water tower: an atmospheric perspective. *Geophys. Res. Lett.* **35**, L20815 (2008).
2. Immerzeel, W. W. et al. Importance and vulnerability of the world's water towers. *Nature* **577**, 364–369 (2020).
3. Yao, T. et al. The imbalance of the Asian water tower. *Nat. Rev. Earth Environ.* **3**, 618–632 (2022).
4. Ehlers, T. A. et al. Past, present, and future geo-biosphere interactions on the Tibetan Plateau and implications for permafrost. *Earth Sci. Rev.* **234**, 104197 (2022).
5. United Nations Environment Programme. *A Scientific Assessment of the Third Pole Environment* (The United Nations Environment Programme (UNEP), 2022).
6. Su, B. et al. Mismatch between the population and meltwater changes creates opportunities and risks for global glacier-fed basins. *Sci. Bull.* **67**, 9–12 (2022).
7. Immerzeel, W. W., van Beek, L. P. H. & Bierkens, M. F. P. Climate change will affect the Asian Water Towers. *Science* **328**, 1382–1385 (2010).

8. Mountain Research Initiative EDW Working Group. Elevation-dependent warming in mountain regions of the world. *Nat. Clim. Chang.* **5**, 424–430 (2015).

9. Kuang, X. & Jiao, J. J. Review on climate change on the Tibetan Plateau during the last half century. *J. Geophys. Res. Atmos.* **121**, 3979–4007 (2016).

10. Yang, M., Wang, X., Pang, G., Wan, G. & Liu, Z. The Tibetan Plateau cryosphere: Observations and model simulations for current status and recent changes. *Earth Sci. Rev.* **190**, 353–369 (2019).

11. Zhang, G., Yao, T., Xie, H., Zhang, K. & Zhu, F. Lakes' state and abundance across the Tibetan Plateau. *Chin. Sci. Bull.* **59**, 3010–3021 (2014).

12. Song, C., Huang, B., Richards, K., Ke, L. & Hien Phan, V. Accelerated lake expansion on the Tibetan Plateau in the 2000s: induced by glacial melting or other processes? *Water Resour. Res.* **50**, 3170–3186 (2014).

13. Lei, Y. & Yang, K. The cause of rapid lake expansion in the Tibetan Plateau: climate wetting or warming? *Wiley Interdiscip. Rev. Water* **4**, e1236 (2017).

14. Cui, T. et al. Non-monotonic changes in Asian Water Towers' streamflow at increasing warming levels. *Nat. Commun.* **14**, 1176 (2023).

15. Yang, M. et al. Desertification and its relationship with permafrost degradation in Qinghai-Xizang (Tibet) plateau. *Cold Reg. Sci. Technol.* **39**, 47–53 (2004).

16. Cheng, G. & Wu, T. Responses of permafrost to climate16 change and their environmental significance, Qinghai-Tibet Plateau. *J. Geophys. Res. Earth Surf.* **112**, F02S03 (2007).

17. Mu, C. et al. The status and stability of permafrost carbon on the Tibetan Plateau. *Earth Sci. Rev.* **211**, 103433 (2020).

18. Lamsal, P., Kumar, L., Shabani, F. & Atreya, K. The greening of the Himalayas and Tibetan Plateau under climate change. *Glob. Planet. Chang.* **159**, 77–92 (2017).

19. Li, R., Gao, Y., Chen, D., Zhang, Y. & Li, S. Contrasting vegetation changes in dry and humid regions of the Tibetan Plateau over recent decades. *Sci. Cold Arid Reg.* **10**, 482–492 (2018).

20. Wu, B. Weakening of Indian summer monsoon in recent decades. *Adv. Atmos. Sci.* **22**, 21–29 (2005).

21. Yao, T. et al. Different glacier status with atmospheric circulations in Tibetan Plateau and surroundings. *Nat. Clim. Chang.* **2**, 663–667 (2012).

22. Ma, J., Ren, H., Cai, M. & Huang, J. Seasonally evolving trends explain the north-south dipole pattern observed in Tibetan Plateau precipitation. *Geophys. Res. Lett.* **50**, e2023GL104891 (2023).

23. Jiang, J. et al. Precipitation regime changes in High Mountain Asia driven by cleaner air. *Nature* **623**, 544–549 (2023).

24. Son, J. H., Seo, K. H. & Wang, B. Dynamical control of the Tibetan Plateau on the East Asian summer monsoon. *Geophys. Res. Lett.* **46**, 7672–7679 (2019).

25. Yang, M., Yao, T., Wang, H., Tian, L. & Gou, X. Estimating the criterion for determining water vapour sources of summer precipitation on the northern Tibetan Plateau. *Hydrol. Process* **20**, 505–513 (2006).

26. Kurita, N. & Yamada, H. The role of local moisture recycling evaluated using stable isotope data from over the middle of the Tibetan Plateau during the monsoon season. *J. Hydrometeorol.* **9**, 760–775 (2008).

27. An, W. et al. Enhanced recent local moisture recycling on the northwestern Tibetan Plateau deduced from ice core deuterium excess records. *J. Geophys. Res. Atmos.* **122**, 12541–12556 (2017).

28. Curio, J., Maussion, F. & Scherer, D. A 12-year high-resolution climatology of atmospheric water transport over the Tibetan Plateau. *Earth Syst. Dyn.* **6**, 109–124 (2015).

29. Zhang, C., Tang, Q. & Chen, D. Recent changes in the moisture source of precipitation over the Tibetan Plateau. *J. Clim.* **30**, 1807–1819 (2017).

30. Xu, Y. & Gao, Y. Quantification of evaporative sources of precipitation and its changes in the southeastern Tibetan Plateau and Middle Yangtze River basin. *Atmosphere* **10**, 428 (2019).

31. Guo, L. et al. Moisture sources for East Asian precipitation: mean seasonal cycle and interannual variability. *J. Hydrometeorol.* **20**, 657–672 (2019).

32. Zhang, C. Moisture source assessment and the varying characteristics for the Tibetan Plateau precipitation using TRMM. *Environ. Res. Lett.* **15**, 104003 (2020).

33. Zhao, Y., Zhou, T., Li, P., Furtado, K. & Zou, L. Added value of a convection permitting model in simulating atmospheric water cycle over the Asian Water Tower. *J. Geophys. Res. Atmos.* **126**, e2021JD034788 (2021).

34. Zhao, Y. & Zhou, T. Interannual variability of precipitation recycle ratio over the Tibetan Plateau. *J. Geophys. Res. Atmos.* **126**, e2020JD033733 (2021).

35. He, Y. et al. The mechanism of increasing summer water vapor over the Tibetan Plateau. *J. Geophys. Res. Atmos.* **126**, e2020JD034166 (2021).

36. Li, X., Wu, P., Ding, Y., Liu, Y. & Li, Q. Spatial-temporal variation of precipitation recycling over the Tibetan Plateau under climate warming. *Atmos. Res.* **280**, 106431 (2022).

37. Li, Y. et al. Contributions of moisture sources to precipitation in the major drainage basins in the Tibetan Plateau. *Sci. China Earth Sci.* **65**, 1088–1103 (2022).

38. Gao, Y., Chen, F., Miguez-Macho, G. & Li, X. Understanding precipitation recycling over the Tibetan Plateau using tracer analysis with WRF. *Clim. Dyn.* **55**, 2921–2937 (2020).

39. Deng, H. & Ji, Z. Warming and Wetting will continue over the Tibetan Plateau in the Shared Socioeconomic Pathways. *PLoS ONE* **18**, e0289589 (2023).

40. Gillett, N. P. et al. The Detection and Attribution Model Intercomparison Project (DAMIP v1.0) contribution to CMIP6. *Geosci. Model Dev.* **9**, 3685–3697 (2016).

41. O'Neill, B. C. et al. The Scenario Model Intercomparison Project (ScenarioMIP) for CMIP6. *Geosci. Model Dev.* **9**, 3461–3482 (2016).

42. Yao, T. et al. A review of climatic controls on δ18O in precipitation over the Tibetan Plateau: observations and simulations. *Rev. Geophys.* **51**, 525–548 (2013).

43. Zhang, C. et al. Quantifying precipitation moisture contributed by different atmospheric circulations across the Tibetan Plateau. *J. Hydrol.* **628**, 130517 (2024).

44. Pisso, I. et al. The Lagrangian particle dispersion model FLEXPART version 10.4. *Geosci. Model Dev.* **12**, 4955–4997 (2019).

45. Sodemann, H., Schwierz, C. & Wernli, H. Interannual variability of Greenland winter precipitation sources: Lagrangian moisture diagnostic and North Atlantic Oscillation influence. *J. Geophys. Res. Atmos.* **113**, 1–17 (2008).

46. Sun, B. & Wang, H. Moisture sources of semiarid grassland in China using the Lagrangian particle model FLEXPART. *J. Clim.* **27**, 2457–2474 (2014).

47. Ma, M., Tang, J., Ou, T. & Chen, D. Contribution of recycled and external advected moisture to precipitation and its inter-annual variation over the Tibetan Plateau. *J. Geophys. Res. Atmos.* **129**, e2023JD040230 (2024).

48. Joseph, P. V., Sooraj, K. P. & RAJAN, C. K. The summer monsoon onset process over South Asia and an objective method for the date of monsoon onset over Kerala. *Int. J. Climatol.* **26**, 1871–1893 (2006).

49. Wang, B., Ding, Q. & Joseph, P. V. Objective definition of the Indian summer monsoon onset*. *J. Clim.* **22**, 3303–3316 (2009).

50. Tuinenburg, O. A., Theeuwen, J. J. E. & Staal, A. High-resolution global atmospheric moisture connections from evaporation to precipitation. *Earth Syst. Sci. Data* **12**, 3177–3188 (2020).

51. Cheng, T. F. & Lu, M. Global Lagrangian tracking of continental precipitation recycling, footprints, and cascades. *J. Clim.* **36**, 1923–1941 (2023).

52. Kuang, X. & Zhang, Y. Seasonal variation of the East Asian Subtropical Westerly Jet and its association with the heating field over East Asia. *Adv. Atmos. Sci.* **22**, 831–840 (2005).

53. Schiemann, R., Lüthi, D. & Schär, C. Seasonality and interannual variability of the westerly jet in the Tibetan Plateau Region*. *J. Clim.* **22**, 2940–2957 (2009).

54. Dai, L., Cheng, T. F., Wang, B. & Lu, M. Subseasonal features of the Indian monsoon. *J. Clim.* **36**, 7199–7211 (2023).

55. Zhang, C. et al. Moisture source changes contributed to different precipitation changes over the northern and southern Tibetan Plateau. *J. Hydrometeorol.* **20**, 217–229 (2019).

56. Wang, B. & LinHo, Rainy season of the Asian-Pacific summer monsoon. *J. Clim.* **15**, 386–398 (2002).

57. Ding, Y. & Chan, J. C. L. The East Asian summer monsoon: an overview. *Meteorol. Atmos. Phys.* **89**, 117–142 (2005).

58. Cheng, T. F., Lu, M. & Dai, L. The zonal oscillation and the driving mechanisms of the extreme western North Pacific subtropical high and its impacts on East Asian summer precipitation. *J. Clim.* **32**, 3025–3050 (2019).

59. Dai, L., Cheng, T. F. & Lu, M. Summer monsoon rainfall patterns and predictability over southeast China. *Water Resour. Res.* **56**, 1–21 (2020).

60. Zemp, D. C. et al. On the importance of cascading moisture recycling in South America. *Atmos. Chem. Phys.* **14**, 13337–13359 (2014).

61. Fremme, A. & Sodemann, H. The role of land and ocean evaporation on the variability of precipitation in the Yangtze River valley. *Hydrol. Earth Syst. Sci.* **23**, 2525–2540 (2019).

62. Chen, X. et al. A doubled increasing trend of evapotranspiration on the Tibetan Plateau. *Sci. Bull.* **69**, 1980–1990 (2024).

63. Eltahir, E. A. B. & Bras, R. L. Precipitation recycling. *Rev. Geophys.* **34**, 367–378 (1996).

64. Vecchi, G. A. et al. Weakening of tropical Pacific atmospheric circulation due to anthropogenic forcing. *Nature* **441**, 73–76 (2006).

65. Seager, R., Naik, N. & Vecchi, G. A. Thermodynamic and dynamic mechanisms for large-scale changes in the hydrological cycle in response to global warming. *J. Clim.* **23**, 4651–4668 (2010).

66. Tokinaga, H., Xie, S.-P., Deser, C., Kosaka, Y. & Okumura, Y. M. Slowdown of the Walker circulation driven by tropical Indo-Pacific warming. *Nature* **491**, 439–443 (2012).

67. Chadwick, R., Boutle, I. & Martin, G. Spatial patterns of precipitation change in CMIP5: Why the rich do not get richer in the tropics. *J. Clim.* **26**, 3803–3822 (2013).

68. Kjellsson, J. Weakening of the global atmospheric circulation with global warming. *Clim. Dyn.* **45**, 975–988 (2015).

69. Kossin, J. P. A global slowdown of tropical-cyclone translation speed. *Nature* **558**, 104–107 (2018).

70. Held, I. M. & Soden, B. J. Robust responses of the hydrological cycle to global warming. *J. Clim.* **19**, 5686–5699 (2006).

71. Trenberth, K. E. & Guillemot, C. J. Evaluation of the global atmospheric moisture budget as seen from analyses. *J. Clim.* **8**, 2255–2272 (1995).

72. Dai, L., Cheng, T. F. & Lu, M. Anthropogenic warming disrupts intraseasonal monsoon stages and brings dry-get-wetter climate in future East Asia. *npj Clim. Atmos. Sci.* **5**, 11 (2022).

73. Dirmeyer, P. A., Schlosser, C. A. & Brubaker, K. L. Precipitation, recycling, and land memory: an integrated analysis. *J. Hydrometeorol.* **10**, 278–288 (2009).

74. Dirmeyer, P. A., Brubaker, K. L. & DelSole, T. Import and export of atmospheric water vapor between nations. *J. Hydrol.* **365**, 11–22 (2009).

75. Zhou, S. et al. Soil moisture–atmosphere feedbacks mitigate declining water availability in drylands. *Nat. Clim. Chang.* **11**, 38–44 (2021).

76. Wang, B., Jin, C. & Liu, J. Understanding future change of global monsoons projected by CMIP6 models. *J. Clim.* **33**, 6471–6489 (2020).

77. Feng, X., Liu, C., Rasmussen, R. & Fan, G. A 10-yr climatology of Tibetan Plateau vortices with NCEP climate forecast system reanalysis. *J. Appl. Meteorol. Climatol.* **53**, 34–46 (2014).

78. Zhao, Y., Lu, M., Chen, D. & Zhang, L. Understanding the weakening patterns of inner Tibetan plateau vortices. *Environ. Res. Lett.* **19**, 064076 (2024).

79. Zhang, Q. et al. Oceanic climate changes threaten the sustainability of Asia's water tower. *Nature* **615**, 87–93 (2023).

80. Wang, Z., Lei, Y., Che, H., Wu, B. & Zhang, X. Aerosol forcing regulating recent decadal change of summer water vapor budget over the Tibetan Plateau. *Nat. Commun.* **15**, 2233 (2024).

81. Zhang, H. & Gao, Y. Projected changes in precipitation recycling over the Tibetan Plateau based on a global and regional climate model. *J. Hydrometeorol.* **22**, 2633–2644 (2021).

82. Dong, W. et al. Summer rainfall over the southwestern Tibetan Plateau controlled by deep convection over the Indian subcontinent. *Nat. Commun.* **7**, 10925 (2016).

83. Fremme, A., Hezel, P. J., Seland, Ø. & Sodemann, H. Model-simulated hydroclimate in the East Asian summer monsoon region during past and future climate: a pilot study with a moisture source perspective. *Weather Clim. Dyn.* **4**, 449–470 (2023).

84. Numaguti, A. Origin and recycling processes of precipitating water over the Eurasian continent: experiments using an atmospheric general circulation model. *J. Geophys. Res. Atmos.* **104**, 1957–1972 (1999).

85. Läderach, A. & Sodemann, H. A revised picture of the atmospheric moisture residence time. *Geophys. Res. Lett.* **43**, 924–933 (2016).

86. Tuinenburg, O. A. & Staal, A. Tracking the global flows of atmospheric moisture. *Hydrol. Earth Syst. Sci. Discuss.* **24**, 2419–2435 (2020).

87. Goessling, H. F. & Reick, C. H. On the 'well-mixed' assumption and numerical 2-D tracing of atmospheric moisture. *Atmos. Chem. Phys.* **13**, 5567–5585 (2013).

88. van der Ent, R. J. & Savenije, H. H. G. Length and time scales of atmospheric moisture recycling. *Atmos. Chem. Phys.* **11**, 1853–1863 (2011).

89. Allen, S. K., Zhang, G., Wang, W., Yao, T. & Bolch, T. Potentially dangerous glacial lakes across the Tibetan Plateau revealed using a large-scale automated assessment approach. *Sci. Bull.* **64**, 435–445 (2019).

90. Zheng, G. et al. Increasing risk of glacial lake outburst floods from future Third Pole deglaciation. *Nat. Clim. Chang.* **11**, 411–417 (2021).

91. Wu, G. et al. Tibetan Plateau climate dynamics: recent research progress and outlook. *Natl Sci. Rev.* **2**, 100–116 (2015).

92. Lenton, T. M. et al. Tipping elements in the Earth's climate system. *Proc. Natl Acad. Sci. USA* **105**, 1786–1793 (2008).

93. Armstrong McKay, D. I. et al. Exceeding 1.5 °C global warming could trigger multiple climate tipping points. *Science* **377**, eabn7950 (2022).

94. Laloyaux, P. et al. CERA-20C: a coupled reanalysis of the twentieth century. *J. Adv. Model Earth Syst.* **10**, 1172–1195 (2018).

95. Lehner, B., Verdin, K. & Jarvis, A. New global hydrography derived from spaceborne elevation data. *EOS* **89**, 93–94 (2008).

96. Hersbach, H. et al. The ERA5 global reanalysis. *Q. J. R. Meteorol. Soc.* **146**, 1999–2049 (2020).

97. Wang, X., Tolksdorf, V., Otto, M. & Scherer, D. WRF-based dynamical downscaling of ERA5 reanalysis data for High Mountain Asia: Towards a new version of the High Asia Refined analysis. *Int. J. Climatol.* **41**, 743–762 (2021).

98. Ou, T. et al. Simulation of summer precipitation diurnal cycles over the Tibetan Plateau at the gray-zone grid spacing for cumulus parameterization. *Clim. Dyn.* **54**, 3525–3539 (2020).

99. Ou, T. et al. Wet bias of summer precipitation in the northwestern Tibetan Plateau in ERA5 is linked to overestimated lower-level southerly wind over the plateau. *Clim. Dyn.* **61**, 2139–2153 (2023).

100. Adler, R. et al. The Global Precipitation Climatology Project (GPCP) monthly analysis (New Version 2.3) and a review of 2017 global precipitation. *Atmosphere* **9**, 138 (2018).

101. Schneider, U. et al. Evaluating the hydrological cycle over land using the newly-corrected precipitation climatology from the global precipitation Climatology Centre (GPCC). *Atmosphere* **8**, 52 (2017).

102. Harris, I., Osborn, T. J., Jones, P. & Lister, D. Version 4 of the CRU TS monthly high-resolution gridded multivariate climate dataset. *Sci. Data* **7**, 109 (2020).

103. Miralles, D. G. et al. Global land-surface evaporation estimated from satellite-based observations. *Hydrol. Earth Syst. Sci.* **15**, 453–469 (2011).

104. Martens, B. et al. GLEAM v3: satellite-based land evaporation and root-zone soil moisture. *Geosci. Model Dev.* **10**, 1903–1925 (2017).

105. Morice, C. P. et al. An Updated assessment of near-surface temperature change from 1850: the HadCRUT5 Data Set. *J. Geophys. Res. Atmos.* **126**, e2019JD032361 (2021).

106. Huffman, G. J., Stocker, E. F., Bolvin, D. T., Nelkin, E. J. & Tan, J. *GPM IMERG Early Precipitation L3 1 Day 0.1 Degree x 0.1 Degree V06* (Goddard Earth Sciences Data and Information Services Center (GES DISC), 2019).

107. Xie, P. et al. Reprocessed, bias-corrected CMORPH global high-resolution precipitation estimates from 1998. *J. Hydrometeorol.* **18**, 1617–1641 (2017).

108. Wei, G. et al. Comprehensive evaluation of GPM-IMERG, CMORPH, and TMPA precipitation products with gauged rainfall over mainland China. *Adv. Meteorol.* **2018**, 1–18 (2018).

109. Liu, Z. Comprehensive evaluation of high-resolution satellite precipitation products over the Qinghai–Tibetan Plateau using the new ground observation network. *Remote Sens.* **15**, 3381 (2023).

110. Eyring, V. et al. Overview of the Coupled Model Intercomparison Project Phase 6 (CMIP6) experimental design and organization. *Geosci. Model Dev.* **9**, 1937–1958 (2016).

111. Tipka, A., Haimberger, L. & Seibert, P. Flex_extract v7.1.2 - A software package to retrieve and prepare ECMWF data for use in FLEXPART. *Geosci. Model Dev.* **13**, 5277–5310 (2020).

112. Hoffmann, L. et al. From ERA-Interim to ERA5: the considerable impact of ECMWF's next-generation reanalysis on Lagrangian transport simulations. *Atmos. Chem. Phys.* **19**, 3097–3214 (2019).

113. Tuinenburg, O. A. & Staal, A. Tracking the global flows of atmospheric moisture and associated uncertainties. *Hydrol. Earth Syst. Sci.* **24**, 2419–2435 (2020).

114. van der Ent, R. J., Tuinenburg, O. A., Knoche, H. R., Kunstmann, H. & Savenije, H. H. G. Should we use a simple or complex model for moisture recycling and atmospheric moisture tracking? *Hydrol. Earth Syst. Sci.* **17**, 4869–4884 (2013).

115. Dominguez, F., Hu, H. & Martinez, J. A. Two-layer dynamic recycling model (2L-DRM): learning from moisture tracking models of different complexity. *J. Hydrometeorol.* **21**, 3–16 (2020).

116. Brubaker, K. L., Entekhabi, D. & Eagleson, P. S. Estimation of continental precipitation recycling. *J. Clim.* **6**, 1077–1089 (1993).

117. Dominguez, F. et al. Impact of atmospheric moisture storage on precipitation recycling. *J. Clim.* **19**, 1513–1530 (2006).

118. van der Ent, R. J., Savenije, H. H. G., Schaefli, B. & Steele-Dunne, S. C. Origin and fate of atmospheric moisture over continents. *Water Resour. Res.* **46**, 1–12 (2010).

119. Cheng, T. F. & Lu, M. Moisture source-receptor network of the East Asian summer monsoon land regions and the associated atmospheric steerings. *J. Clim.* **33**, 9213–9231 (2020).

120. Cheng, T. F., Lu, M. & Dai, L. Moisture channels and pre-existing weather systems for East Asian rain belts. *npj Clim. Atmos. Sci.* **4**, 32 (2021).

121. Stohl, A. & James, P. A Lagrangian analysis of the atmospheric branch of the global water cycle: Part 1: method description, validation, and demonstration for the August 2002 flooding in central Europe. *J. Hydrometeorol.* **5**, 656–678 (2004).

122. Lettau, H., Lettau, K. & Molion, L. C. B. Amazonia's hydrologic cycle and the role of atmospheric recycling in assessing deforestation effects. *Mon. Weather Rev.* **107**, 227–238 (1979).

123. Adams, D. K. & Comrie, A. C. The North American Monsoon. *Bull. Am. Meteorol. Soc.* **78**, 2197–2213 (1997).

124. Hu, H. & Dominguez, F. Evaluation of oceanic and terrestrial sources of moisture for the North American monsoon using numerical models and precipitation stable isotopes. *J. Hydrometeorol.* **16**, 19–35 (2015).

125. Vera, C. et al. Toward a unified view of the American monsoon systems. *J. Clim.* **19**, 4977–5000 (2006).

126. Montini, T. L., Jones, C. & Carvalho, L. M. V. The South American low-level jet: a new climatology, variability, and changes. *J. Geophys. Res. Atmos.* **124**, 1200–1218 (2019).

127. Hendon, H. H. & Liebmann, B. A composite study of onset of the Australian summer monsoon. *J. Atmos. Sci.* **47**, 2227–2240 (1990).

128. Cheng, T. F., Lu, M., Wang, B. & Dai, L. A fresh view of the Asian-Australian monsoon complexity: The Intertropical Convective Cell (ITCC) framework. *J. Geophys. Res. Atmos.* **129**, e2023JD039498 (2024).

129. Dai, L., Cheng, T. F. & Lu, M. Define East Asian monsoon annual cycle via a self-organizing map-based approach. *Geophys. Res. Lett.* **48**, e2020GL089542 (2021).

130. Wang, W., Zhou, W., Wang, X., Fong, S. K. & Leong, K. C. Summer high temperature extremes in Southeast China associated with the East Asian jet stream and circumglobal teleconnection. *J. Geophys. Res. Atmos.* **118**, 8306–8319 (2013).

131. Cheng, T. F., Dong, Q., Dai, L. & Lu, M. A dual regime of mesoscale convective systems in the East Asian monsoon annual cycle. *J. Geophys. Res. Atmos.* **127**, e2022JD036523 (2022).

132. Cheng, T. F., Chen, D., Wang, B., Ou, T. & Lu, M. A 40-year moisture source data for Tibetan Plateau precipitation using a 3D Lagrangian approach [Dataset]. Zenodo https://doi.org/10.5281/zenodo.11479499 (2024).

133. Pawlowicz, R. M. Map: a mapping package for Matlab (Version 1.4m) [Software]. www.eoas.ubc.ca/~rich/map.html (2020).

Acknowledgements

Author contributions

T.F.C. contributed to the conceptualization, methodology, investigation, visualization, original draft, and revision of the manuscript. D.C. contributed to the conceptualization, investigation, supervision of the project, and revision of the manuscript. B.W. contributed to the methodology, investigation, and revision of the manuscript. T.O. contributed to the

methodology and revision of the manuscript. M.L. contributed to the conceptualization, supervision of the project, and revision of the manuscript.

Competing interests

The authors declare no competing interests.

Additional information

Supplementary information The online version contains supplementary material available at
https://doi.org/10.1038/s43247-024-01563-9.

Correspondence and requests for materials should be addressed to Tat Fan Cheng or Mengqian Lu.

Peer review information *Communications Earth & Environment* thanks He Yongli and the other, anonymous, reviewer(s) for their contribution to the peer review of this work. Primary Handling Editors: Heike Langenberg. A peer review file is available.

Reprints and permissions information is available at
http://www.nature.com/reprints

Publisher's note Springer Nature remains neutral with regard to jurisdictional claims in published maps and institutional affiliations.